Traveling-Wave Photodetectors With High Power–Bandwidth and Gain–Bandwidth Product Performance

Daniel Lasaosa, Jin-Wei Shi, Donato Pasquariello, Kian-Giap Gan, Ming-Chun Tien, Hsu-Hao Chang, Shi-Wei Chu, Chi-Kuang Sun, *Senior Member, IEEE*, Yi-Jen Chiu, and John E. Bowers, *Fellow, IEEE*

Invited Paper

***Abstract*—Traveling-wave photodetectors (TWPDs) are an attractive way to simultaneously maximize external quantum efficiency, electrical bandwidth, and maximum unsaturated output power. We review recent advances in TWPDs. Record high-peak output voltage together with ultrahigh-speed performance has been observed in low-temperature-grown GaAs (LTG-GaAs)-based metal–semiconductor–metal TWPDs at the wavelengths of 800 and 1300 nm. An approach to simultaneously obtain high bandwidth and high external efficiency is a traveling-wave amplifier-photodetector (TAP detector) that combines gain and absorption in either a sequential or simultaneous traveling-wave structure.**

***Index Terms*—Amplifier, GaAs, high speed, InGaAsP, photodetector, traveling wave.**

I. Introduction

PROPOSED communication systems at 40 Gb/s, 160 Gb/s, and beyond require photodetectors (PDs) with large bandwidths, high quantum efficiency, and high saturation powers. Unfortunately, conventional surface normal photodetectors are limited to bandwidth efficiency products of typically 30 GHz [1], [2] and saturation powers of typically 10 dBm [2]. Resonant cavities [3] or waveguide photodetectors (WGPD) [1], [2], [4], [5] are needed to achieve higher bandwidth efficiency products. To achieve the highest performance, traveling wave structures are required [6]–[10]. These structures combine controlled impedance lines with long absorption regions to achieve extremely large bandwidth efficiency products and high saturation powers.

Two approaches to increase the responsivity are optical gain, described as follows, and avalanche gain [11]–[19]. Approaches to increase the saturation power are increasing the carrier velocity using a uni-traveling carrier PD (UTC-PD) [2], [20], [21] or reducing the optical modal absorption constants and increasing absorption lengths in traveling-wave photodetector (TWPD), WGPD, or periodic traveling-wave photodetector (P-TWPD) structures [10], [22]–[24]. Recently, several research groups have successfully demonstrated the TWPDs with high speed and high-saturation power performance in the 1.55-μm wavelength regime for the applications of analog or digital fiber communication [25], [26].

In this paper, we review recent work on TWPDs with high gain–bandwidth and high saturation power–bandwidth product performances. By utilizing the short carrier trapping time of low-temperature-grown GaAs (LTG-GaAs) and the superior microwave guiding structure of metal–semiconductor–metal TWPD (MSM-TWPD) [27], record saturation power-bandwidth product performances of LTG-GaAs-based MSM-TWPD have been demonstrated in short ($\sim$800 nm) [28] and long ($\sim$ 1300 nm) telecommunication wavelengths regimes [29]. Distinct bandwidth degradation behavior, which can be attributed to hot electron effects of photogenerated carriers [30], [31], have also been observed. By utilizing the good speed and output power performances of MSM-TWPD, we have also demonstrated the novel structure of an LTG-GaAs-based terahertz photonic transmitter [32]. By utilizing the fully distributed microwave guiding property of the MSM-TWPD, short carrier-trapping time of LTG-GaAs, and a membrane antenna structure, high conversion efficiency ($\sim 1.1\times 10^{-3}$) can be achieved at 650-GHz frequency [33].

We have also proposed a novel device, the traveling-wave amplifier photodetector (TAP detector), designed specifically to achieve simultaneously very high gain and ultrafast frequency response, through the distributed combination of optical gain and absorption [34], [35]. This paper describes the theory [35], [36] behind the performance of this device as well as device results in GaAs [37], [38] and InP [38]–[40].

Manuscript received April 1, 2004; revised May 27, 2004.

D. Lasaosa, K.-G. Gan, and J. E. Bowers are with the Department of Electrical and Computer Engineering, University of California, Santa Barbara, CA 93106 USA (e-mail: bowers@ece.ucsb.edu).

J.-W. Shi is with the Department of Electrical Engineering, National Central University, Taoyuan 320, Taiwan, R.O.C.

D. Pasquariello is with Philips Research Laboratories, Eindhoven, The Netherlands.

M.-C. Tien, H.-H. Chang, S.-W. Chu, and C.-K. Sun are with the Department of Electrical Engineering and Graduate Institute of Electro-Optical Engineering, National Taiwan University, Taipei 10617, Taiwan, R.O.C.

Y.-J. Chiu is with the Institute of Electro-Optical Engineering, National Sun Yat-Sen University, Kaohsiung 804, Taiwan, R.O.C.

Digital Object Identifier 10.1109/JSTQE.2004.833963

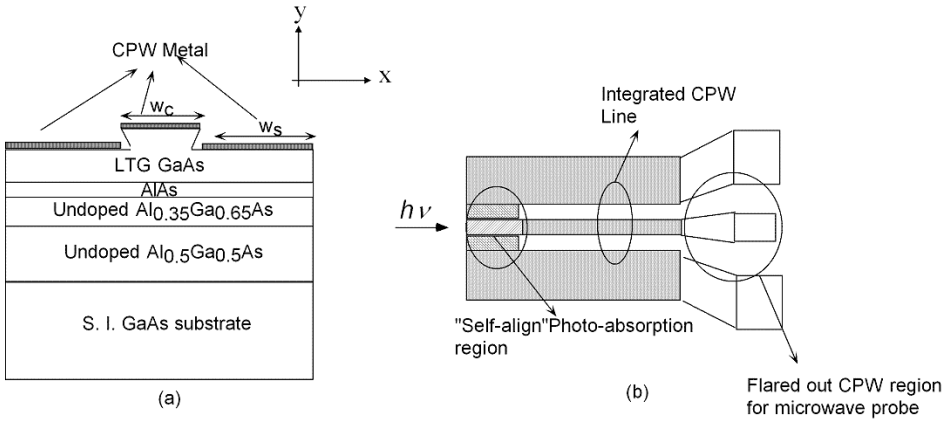

Fig. 1. (a) Cross-sectional diagram and (b) top view of MSM-TWPD. Integrated CPW line is for EO sampling measurement purpose.

II. MSM TWPDs

A. MSM-TWPD Structure

Traveling-wave detectors are attractive because the intrinsic layer can be thin enough that transit time is not a bandwidth limit, and the capacitance is not a bandwidth limit due to the use of a transmission line. MSM detectors are attractive to achieve lower capacitance per unit length and are easier to achieve a 50-Ω transmission line with velocity-matched property [10], which implies the velocity of optical wave and photogenerated microwave signal are almost the same, as compared to the structure of p-i-n detectors [24]. The cross-sectional scheme of a typical MSM-TWPD is shown in Fig. 1(a). The epitaxial structure consists of a thin LTG-GaAs layer (500 nm) for photoabsorption and two AlGaAs layers for optical waveguiding and optical isolation between the GaAs substrate and the LTG-GaAs active layer. A thin (100 Å) AlAs layer is used to avoid As out-diffusion during annealing. The optical waveguiding in the x-direction is achieved by the etched-mesa ridge structure. Three metal stripes are electrodes to collect the photogenerated carriers in LTG-GaAs layer and support a photoexcited microwave guiding mode. By utilizing the self-aligned process, the gap between ground plane (with width w_s) and center stripe (with width w_c) can be shortened to 200–300 nm without E-beam lithography. There are some advantages for the narrow gap width of coplanar waveguide (CPW) line, such as the improvement in internal quantum efficiency of PDs and the reduction in dominant microwave radiation loss in the ultrahigh-frequency regime (several hundreds of gigahertz) [41]. Fig. 1(b) shows the top view of the device. The active region of the photodetector (self-aligned photoabsorption region) is integrated with a CPW line in its output for electrooptical (EO) sampling measurement [42] and dc-biasing purposes.

B. MSM-TWPD Characteristics

The dc I–V and EO sampling measurements described below used mode-locked Ti : sapphire and Cr^{4+} : forsterite lasers as the light sources at short (800 nm) and long (~1230 nm) wavelengths regimes, respectively. The geometry structures of measured MSM-TWPDs at these two wavelengths are the same except that the device absorption lengths for 1230 and 800 nm studies are 70 and 12 μm, respectively, due to different optical

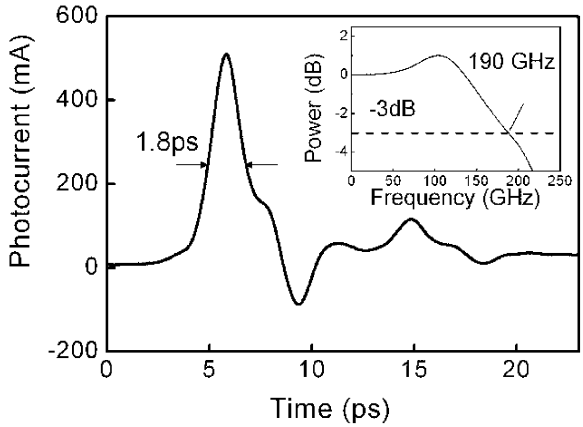

Fig. 2. EO measured transient response of a 12-μm-long MSM-TWPD with high optical excitation energy (71 pJ/pulse) and a fixed high bias voltage (30 V) at the excited wavelength of 800 nm. Inset shows its corresponding frequency domain response by use of fast Fourier transform technique, which shows a 3-dB electrical bandwidth of 190 GHz.

modal absorption constants [28], [29]. Under short wavelength excitation, the value of obtained quantum efficiency is about 8.1% under 15-V dc bias voltage. This value is similar to that of the reported quantum efficiency of LTG-GaAs-based p-i-n TWPD [43]. Fig. 2 shows the EO measured impulse response under high dc bias voltage (30 V) and high optical excitation energy (~71 pJ/pulse) at short wavelength regime. Its corresponding frequency response is given in the inset and shows a 190-GHz electrical bandwidth. We calculated the peak output voltage (V_p) to be about 30 V with ~500 mA peak output photocurrent, by utilizing the collected photogenerated charge per pulse (~2100 fC), the area of the measured impulse response, and the characteristic impedance (~60 Ω) of integrated CPW transmission line. The dc bias voltage (also 30 V) thus limited the maximum output peak voltage due to external circuit saturation effects. The peak voltage V_p (~30 V) and electrical bandwidth (190 GHz) product (5.7 THz-V) is the highest among all the reported ultrahigh-speed PDs, including LTG-GaAs-based p-i-n TWPDs (~1400 fC, 6 ps) [44], MBE annealed MSM-TWPD (~ 1600 fC, 1.5 ps, 220 GHz, 4.4 THz-V) [45], InGaAs-based vertical p-i-n PD (~7.2 ps, 68 fC) [46], GaAs-based p-i-n TWPD (~5.5 ps, 59 fC) [47], unitraveling carrier PD (UTC-PD, ~3.1 ps, 115 GHz, V_p : 1.92 V) [20], and VMDP

(40–50 GHz, V_p : 2.5 V) [48]. This excellent power–bandwidth product of MSM-TWPD is due to the MSM microwave guiding structure but also due to the short carrier trapping time and the high-voltage capability of LTG-GaAs. However, the short carrier trapping time reduces the quantum efficiency in LTG-GaAs-based PDs. Thus, most of the collected carriers travel through extremely short distances where a stronger electric field exists with less space charge screening effect [2], [49].

It is interesting to consider the application of LTG-GaAs-based PDs in the long wavelength communications regime. This GaAs PD is attractive due to its ultrahigh-speed performance, lower cost, and more mature material growth and processing techniques as compared to InP-based devices. The below band-gap absorption in LTG-GaAs is achieved by utilizing a mid-gap defect state to conduct band transitions. However, the small below-bandgap absorption constant results in low quantum efficiency (∼0.6 mA/W) for traditional vertical-illuminated PD structure [50], [51]. However, an MSM-TWPD structure can have reasonable quantum efficiency by properly increasing the device absorption length. The device responsivity under 15-V dc bias was ∼11 mA/W and is much higher than the reported value of (∼0.6 mA/W) vertical-illuminated MSM PDs structure [51]. The peak output voltage (or power) and the electrical bandwidth of an ultrahigh-speed photodetector depend on the applied bias voltage and the illuminated optical power. Fig. 3 shows the EO measured impulse response with its corresponding frequency responses shown in the inset under optimum dc bias voltage (10 V) and optical excitation energy (∼28 pJ/pulse) for maximum V_p-bandwidth product performance at long wavelength regime [29]. The maximum V_p-bandwidth product of 568 GHz-V corresponds to a 160-GHz 3-dB electrical bandwidth and a 3.55-V peak output voltage (with 71-mA peak current and 50-Ω load). Compared with state-of-the-art high-power InP-based UTC-PD [2], [20], our device shows a higher bandwidth and peak-output-voltage product.

As shown in Figs. 2 and 3, although the long wavelength MSM-TWPD has a much longer length, the maximum output V_p is much lower than the case of short wavelength excitation. To understand the nonlinear behavior of LTG-GaAs-based PD under different wavelength excitations (800 versus 1230 nm), we have also performed EO sampling measurements in these two wavelength regimes with different pumping power [30], [31]. Fig. 4 shows the EO measured impulse current responses under 800 nm [Fig. 4(a)] and 1230 nm [Fig. 4(b)] excitations. A to D traces are results under different illumination intensities. Also shown beside the traces are the corresponding collected carrier densities, which can be obtained by dividing the collected charges by the device absorption volumes. The effective device absorption lengths that we used in volume and density calculations are 24 and 12 μm for 1230- and 800-nm wavelength excitation, respectively. The effective device absorption lengths were obtained by comparing photocurrents from different absorption-length devices. For the case of MSM-TWPD, the measured photocurrent will not increase with the absorption length significantly, when its value is over 12 and 24 μm at the measured two wavelengths. We can thus ensure that most of the photogenerated carriers are concentrated on these

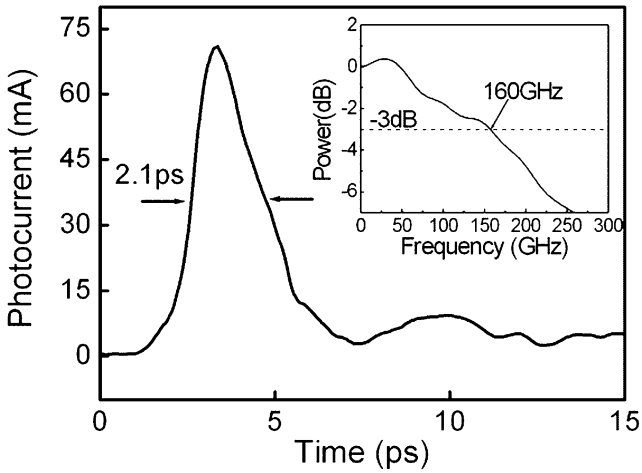

Fig. 3. EO measured transient response of a 70-μm-long MSM-TWPD corresponding to the best V_p-bandwidth product condition at the excited wavelength of 1230 nm. Inset shows its corresponding frequency domain response with fast Fourier transform technique.

lengths (effective absorption volume) instead of real geometric lengths (absorption volume) of devices. In Fig. 4(a), under the condition of shorter absorption length and higher collected carrier density compared to the cases of Fig. 4(b), there is much less broadening in the measured EO traces even with the highest collected carrier density (trace D). However, the traces measured at the 1230-nm wavelength [Fig. 4(b)] show serious broadening with increasing collected carrier densities. The observed nonlinear behavior is opposite the general design concept of high speed/power PDs, which are made to achieve less electrical bandwidth degradation in high output-power regime by reducing the optical modal absorption constant and increasing the device absorption length. Fig. 5(a) and (b) shows the measured impulse full-width at half-maximum (FWHM) under short and long wavelength excitations versus dc bias voltage at different optical illumination powers, respectively [30], [45]. As shown in Fig. 5(a), we can clearly see that in most optical pumping energies, as shown in traces of B ∼ F, an optimal bias point, which will increase with the optical excitation energy, for the fastest device response exists. We attributed this nonlinear behavior to the combination of different physical processes including carrier lifetime increasing [52], defect saturation, and space-charge screening effects [44], [45]. In the low optical excitation regime the dominant bandwidth limiting factor is carrier lifetime increasing and the FWHM increases with the bias voltage due to carrier heating and intervalley scattering [30], [31] instead of the reported coulomb-barrier lowering effect [52], because the electric field in the optical guiding mode center of our device is not high enough to induce this effect significantly [28], [30], [31]. When the photoexcited carrier density increases, the carrier trapping time will increase significantly because defect saturation reduces the carrier capture probability, and the drift time and significant space-charge field of photogenerated carriers start to affect the speed performance of the device. By increasing the dc bias voltage, we can overcome the space-charge field and improve the speed of the device. However, with further increased bias voltage, the FWHM broadens again due to the

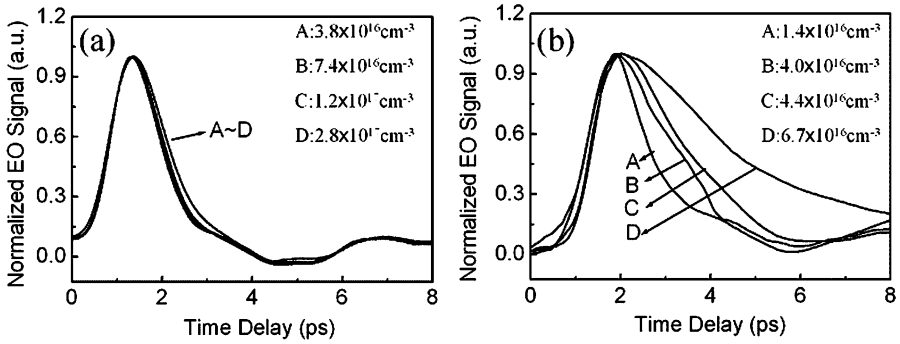

Fig. 4. Normalized E–O sampling traces of LTG-GaAs-based MSM-TWPDs under (a) 800-nm wavelength and (b) 1230-nm wavelength short pulse excitations under different illumination intensities. DC biases were fixed at 10 and 5 V for (a) and (b), respectively.

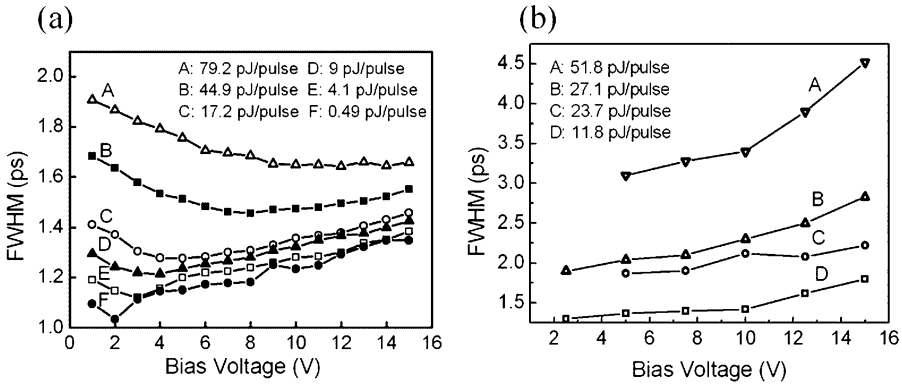

Fig. 5. FWHM of the measured impulse responses versus dc bias voltages with different optical excitation energies under(a) 800-nm and (b) 1230-nm wavelengths excitation. Optical pumping energy for each trace is labeled on the figure.

lifetime increasing effect as discussed before. At Fig. 5(a), these optimal bias points for narrowest FWHM shift toward higher voltages for higher optical pumping energies due to that fact that a higher electric field is needed to overcome the carrier-induced space-charge field. As shown in Fig. 5(b), all the traces show a more serious broadening as compared to the traces of Fig. 5(a). The reduction of the FWHM with the increase in dc bias voltage, as shown in Fig. 5(a), does not happen in the case of long wavelength excitation. These measurement results imply that the dominant bandwidth-limiting factor is the lifetime increasing effect under long wavelength excitation. We attributed the distinct nonlinear behaviors to the different photoabsorption mechanisms under the excitations of these two wavelengths. For 1230-nm subband-gap excitation, carriers in the mid-gap states can be excited into the Γ valley with high excess energy ($\sim$300 meV), which is close to the offset energy ($\sim$310 meV) of the L valley relative to the Γ bottom. These photoexcited electrons will suffer from the intervalley scattering effect (Gunn effect) more easily as compared to the case of short wavelength excitation [30], [31]. This effect should reduce the electron capture rate back to the defect states and cause the broadening of the carrier-lifetime-limited device responses. Based on the above discussion, our observed hot carrier phenomena should also take place in LTG-GaAs-based devices under normal band-to-band excitation with photon energy much larger than the bandgap energy. Serious bandwidth degradation of LTG-GaAs-based photomixers have been observed under $\sim$585-nm wavelength excitation [53].

C. Terahertz Generation

By utilizing the fully distributed microwave guiding property of the MSM-TWPD and a membrane antenna structure, we have also demonstrated a novel terahertz photonic transmitter [32], [33] with high conversion efficiency. Compared with other millimeter- or submillimeter-wave emission techniques such as Gunn diodes [54], p-type Ge-based or quantum cascade terahertz lasers [55], [56], and resonant tunneling diodes [57], photonic transmitters have the advantages of simplicity, compactness, wide tunability, and room temperature operations. To test the performance of our fabricated device, the light source that we used was a mode-locked Ti:sapphire laser with 100-fs optical pulsewidth and 82-MHz repetition rate. By passing the broadband femtosecond optical pulses through etalons, we can increase the repetition rate of the light source to terahertz frequency range and trigger the photonic transmitters by coupling this high-repetition-rate light into the edge-coupled MSM-TWPD [32], [33]. The top view of our device is shown in Fig. 6, which is composed of a MSM-TWPD, a radio frequency (RF) choke filter, and a planar antenna [33]. We adopted a CPW fed slot antenna because it can generate higher power than the spiral antenna in the designed resonant frequency [58] and can be easily integrated with the MSM-TWPD. The RF choke filter, which acts as an inductance [41], avoids the high-frequency ac current (with a resonant frequency of the slot line antenna) leaking into the dc probe pad. We removed the GaAs substrate and mounted the membrane of the fabricated device on a glass substrate, which has a much lower dielectric

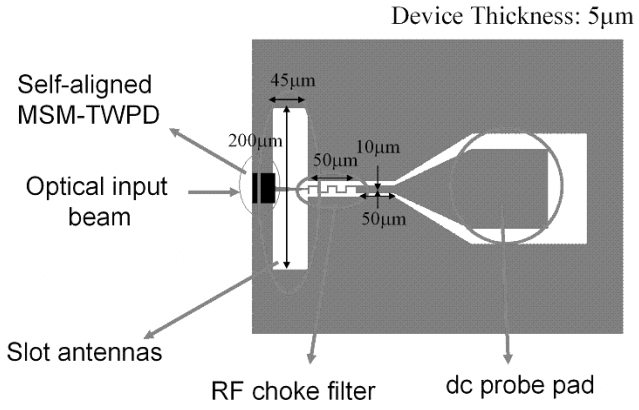

Fig. 6. Structure of the edge-coupled membrane photonic transmitter. Geometric information for the 650-GHz device is provided.

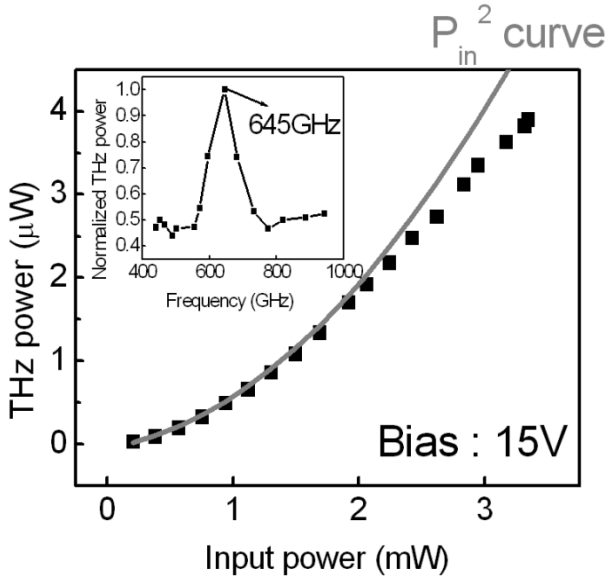

Fig. 7. Measured terahertz output power (solid square) and fitted squared input optical power (solid line) versus input optical power under a fixed dc bias voltage of 15 V.

constant than GaAs substrates and can thus allow the radiation of terahertz energy into the substrate or free space without using a Si lens [32], [33]. Fig. 7 shows the excitation optical power-dependent terahertz output power under a fixed dc bias voltage (15 V) and operating at the resonant frequency of the antenna [32]. The frequency response of the integrated antenna is shown in the inset, which shows a resonance at the designed frequency (∼645 GHz) of the antenna. The external conversion efficiency of our new device at 645-GHz radiation is 0.11%. To our knowledge, this value is the highest reported conversion efficiency of all photonic transmitters with radiation frequency higher than 500 GHz and is 15 times higher than the optimum value that has been reported at a similar radiation frequency [58]. In addition, the trace of fitted squared input optical power (P_{in}^2) shows that the collected terahertz radiation power does not follow a quadric relation with optical excitation power [59], especially in the case of high-power illumination. The observed output power saturation behavior can be attributed to the bandwidth degradation effect as discussed in Fig. 5(a). The edge-coupled structure and high conversion efficiency characteristic of our demonstrated devices are suitable for monolithic integration with a mode-locked semiconductor laser with high repetition rate or a two-wavelength continuous-wave diode laser. The integrated device can act as a compact all solid-state and tunable terahertz radiation source.

III. TAP Detectors

There are three approaches to making traveling wave amplifier photodetectors. One approach is to sequentially combine absorption and gain regions [Fig. 8(a)]. The segments are designed such that the peak local photocurrents remain below saturation levels. Alternatively, gain and absorption can occur simultaneously as the mode travels down the waveguide. These gain and absorption regions can be arranged laterally [Fig. 8(b)] or vertically [Fig. 8(c)]. We will focus on vertical coupled TAP detectors to avoid the scattering and loss associated with the transitions between sequential TAP regions.

A. Qualitative Performance of TAP Detectors With Vertical Coupling

Fig. 8(d) and (e) shows a top view and cross section of TAP detectors with vertical coupling fabricated in GaAs, respectively. This vertically stacked configuration is an improvement over the originally proposed TAP detectors with lateral coupling [34], [35]. Featuring a quantum well-based amplification region and a bulk detection region, a single-epitaxy structure is grown which allows for the separate optimization of gain and absorption regions. Electrical isolation between these two active regions, which would require processes such as implantation, intermixing, and/or regrowth in a structure presenting gain and absorption regions side by side, is obtained in the vertically stacked configuration through bandgap engineering. In this configuration, a parasitic transistor is formed by the stacking of either p-n-p or n-p-n claddings which allow current injection into the amplification active region and photocurrent extraction from the absorption region. The middle cladding, between both active regions, plays the role of the base in this parasitic transistor, while the lower cladding below the gain active region acts as emitter. Carrier confinement in the gain active region reduces the number of carriers injected into the "base." A thick middle cladding ensures that a small fraction of those arriving into the absorption diode, result in the inhibition of transistor action. Simultaneous measurement of the background current in the detection diode and the amplified spontaneous emission (ASE) produced in the amplification region, in the absence of an optical input, confirmed that the fraction of background current produced by the action of this parasitic transistor was in fact negligible for good device design [38].

The EO response of TAP detectors is given by the superposition of the photocurrents generated by three types of modes, exhibiting different behaviors. We denote these three types of modes as "detector modes," "amplifier modes, " and "cladding modes." Detector modes have a large overlap with the absorption region. They are short lived, propagating over short lengths (∼10–50 μm) before being fully absorbed. They are not heavily influenced by the gain in the amplification

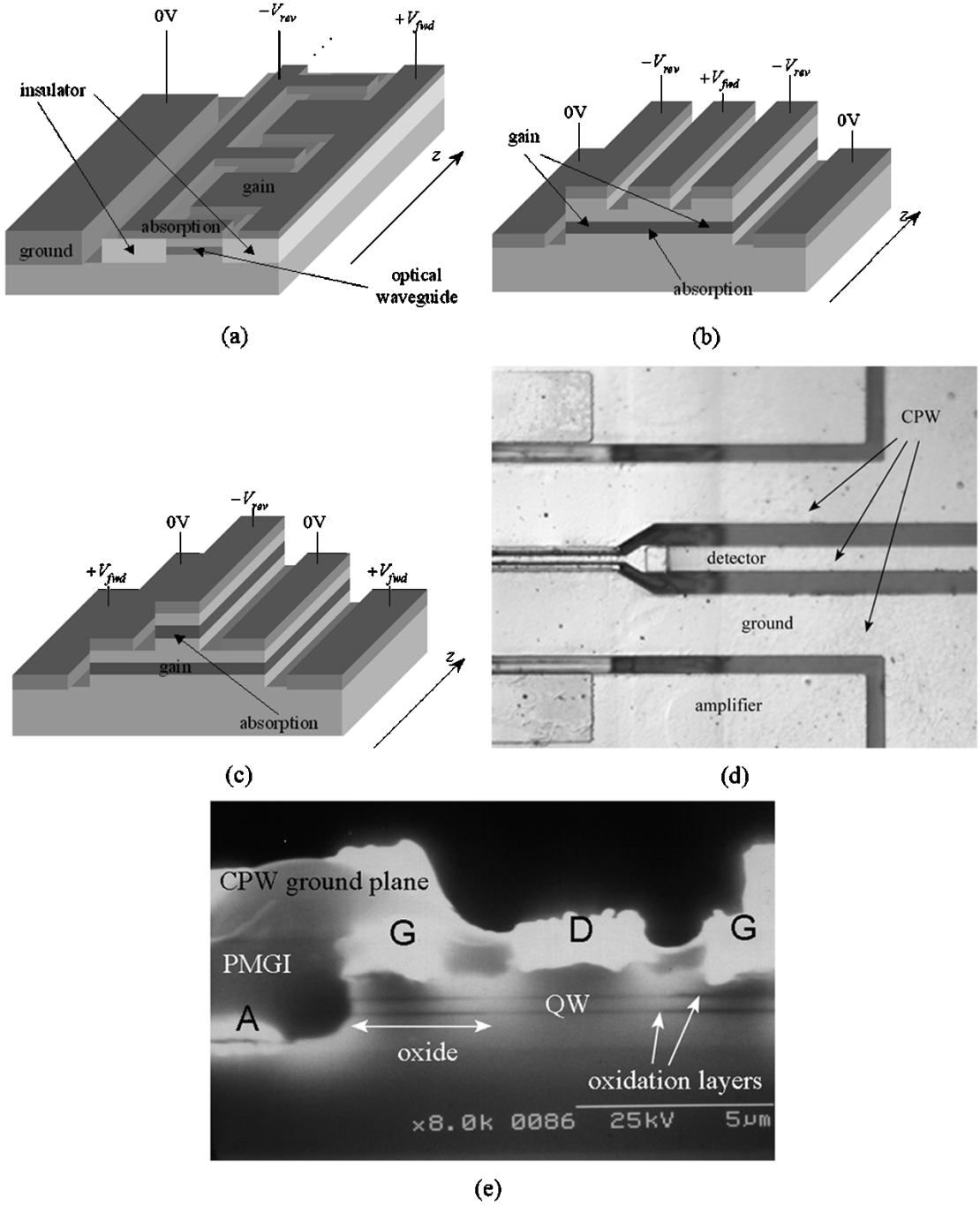

Fig. 8. TAP detectors with (a) sequential gain and absorption along the length of the detector, (b) simultaneous lateral gain and absorption, and (c) simultaneous vertical gain and absorption. (d) Top and (e) end view of fabricated vertical coupled GaAs-based TAP detectors.

region, and their response does not significantly depend on the bias current applied between bottom and middle claddings (bias current injected into the gain diode). They are responsible for generating most of the photocurrent detected when the gain diode is left unbiased. Amplifier modes exhibit a large overlap with the gain region and a smaller overlap with the detection region. These modes may actually reach a zero net gain, through the joint action of amplification, absorption, and loss. This "zero modal gain" situation is, in fact, the most interesting operating point for TAP detectors [34]. They are responsible for most of the photocurrent increase as a higher bias current is injected into the gain diode, thus enabling a higher than 100% external quantum efficiency. Cladding modes reside mostly on the bottom cladding, overlapping partially with the gain region, and barely with the absorption region. These modes experience a relatively large net gain when amplifier modes are close to zero modal gain, producing a large increase in the guided optical power, but barely contributing to the total photocurrent detected. In order to fully understand the behavior of TAP detectors, we need to take into account the simultaneous presence of these three types of modes, together with the measurable photocurrent. We define the measurable

photocurrent at a given gain diode bias current as the difference between the total detection diode current measured in the presence and in the absence of an optical input. As the input optical power increases, stimulated recombination depletes the electrical carriers injected into the gain region at a faster rate, resulting in a lower production of spontaneous emission and ASE for the same gain diode bias current. This results in the measurable photocurrent being, in fact, lower than the actual amount of photocurrent produced [38]. This difference between actual and measurable photocurrent increases as the gain diode saturates and is a direct consequence of the impossibility to separate the detection diode current generated by absorption of either optical input signal, spontaneous emission, or ASE.

B. Experimental Results

With this qualitative background, we can explain the experimental results that are observed. Fig. 9(a) shows the index profile and the mode structure of the TAP detector. Fig. 9(b) shows the measurable photocurrent obtained in the first GaAs TAP detectors with vertical coupling [35], as a function of the vertical displacement of the lensed fiber used to couple light into the device. The lowest photocurrent is obtained for the largest vertical displacement, corresponding to the lowest position of the fiber with respect to the device. At this point, most of the power coupled into the device feeds the cladding mode, and only a small fraction of it is transferred into the amplifier mode. As the displacement is reduced, less optical power is coupled into the cladding mode, resulting in lower competition between signal and ASE for the available gain, with an ensuing increase in the measurable photocurrent. The measurable photocurrent finally decreases again as the fiber is moved above the point which produces optimum coupling into the amplifier mode. At this position (vertical displacement of 0–1 μm), an enhanced coupling of the input signal into the detector mode produces a larger photocurrent when the gain diode is left unbiased, but little improvement is obtained by increasing the gain diode bias current, as little power is coupled into the amplifier mode.

To eliminate the cladding mode, the index of refraction of the bottom cladding was reduced, by increasing its aluminum fractional content from 15%–20% to 25%, and the external quantum efficiency improved to over 200%. The reduction in the device efficiency through competition between ASE and optical signal for the available gain is still clearly shown in Fig. 10, as the measurable efficiency decreases with increasing input optical power. From Figs. 9 and 10, we may therefore conclude that inhibition of parasitic modes that do not overlap with the absorption region does indeed improve TAP detector performance and that further improvements are possible as long as the effect of the competition between ASE and signal is reduced.

C. Advantages of TAP Detectors With Alternating Gain and Absorption

TAP detectors featuring alternating gain and absorption, shown in Fig. 8(a), present *a priori* several advantages over a vertically stacked configuration. The main ones are superior microwave propagation characteristics [34], [35], the possibility to introduce integrated ASE filtering, and the elimination

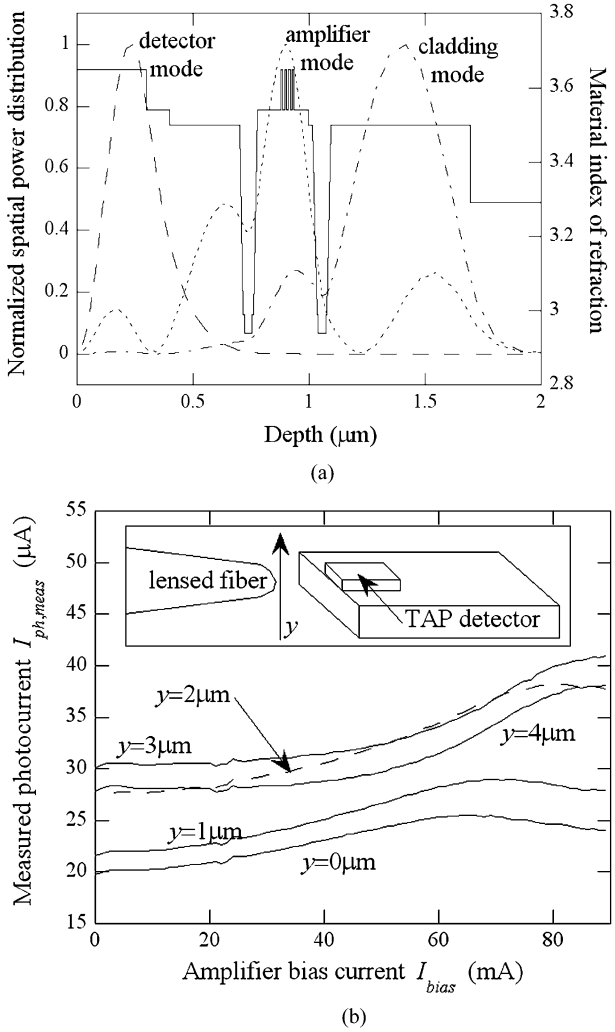

Fig. 9. (a) Refractive index (full line) in the epitaxial structure used to fabricate vertically coupled TAP detectors and simulated guided modes supported: detector mode (dashed line), amplifier mode (dotted line), and cladding mode (dash-dotted line). (b) Measured photocurrent in a 300-μm-long nonantireflective-coated device fabricated on this epitaxial structure as a function of the amplifier bias current, for different vertical displacements of the input coupling lensed fiber y. Incident optical power is 200 μW. Inset shows a schematic representation of the coupling of light input into the device. The y direction is shown. Direction of propagation of light [z direction in Fig. 8(c)] is left to right.

of most of the contribution to the background current from absorption of nonamplified spontaneous emission. The price for these advantages is higher device fabrication complexity. Once the concept of distributed combination of gain and absorption has been demonstrated using the easier-to-fabricate vertically stacked configuration, TAP detectors with alternating gain and absorption are ideal candidates for future performance improvements. Before describing in detail the advantages of one configuration over the other, it is noteworthy to mention that other performance parameters not compared in this paper, such as the external quantum efficiency or generation of background current due to absorption of ASE, are virtually identical in both configurations. This is due to the fact that, conceptually, a stacked configuration is nothing more than a "continuous" version of a TAP detector with alternating gain and absorption, where each differential element of length may be subdivided in

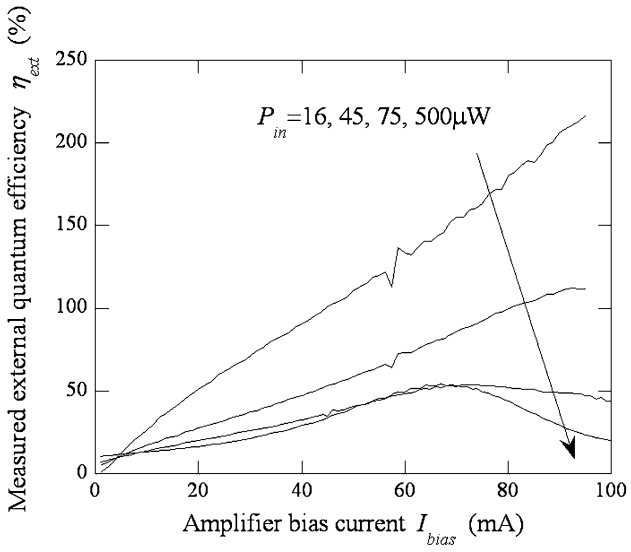

Fig. 10. Measured external quantum efficiency in vertically coupled GaAs-based TAP detectors from an optimized epitaxial structure designed to remove cladding modes, as a function of the amplifier bias current, and for different values of the input optical power. Device length is 200 μm, and its front facet was antireflective coated.

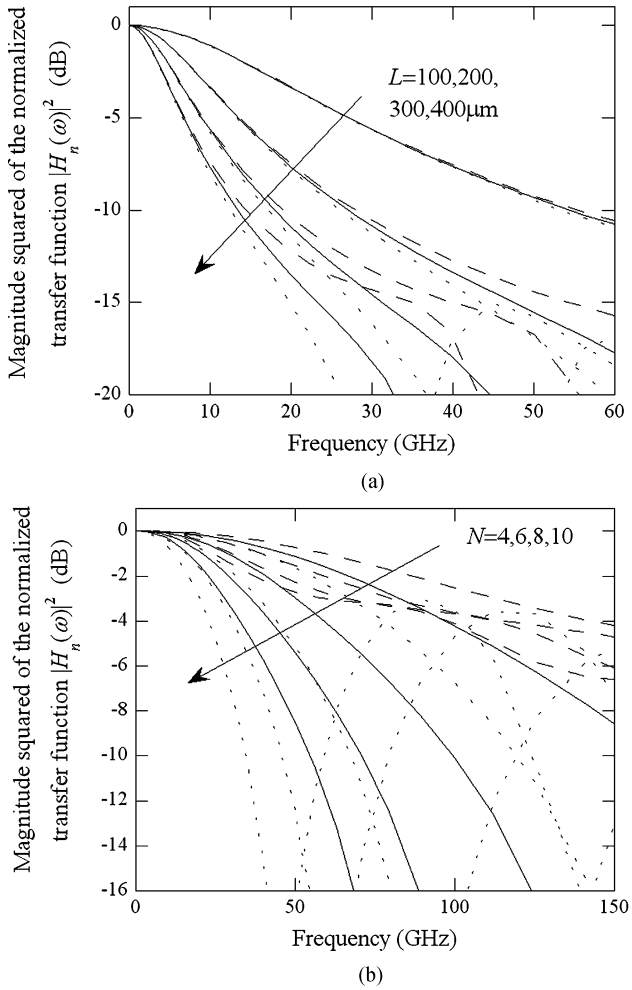

Fig. 11. (a) Simulated frequency response for TAP detectors with vertical coupling for different values of the net gain per unit length Δg and different device lengths L. Δg is 0 (full lines) -20 cm $^{-1}$ (dashed lines), and 20 cm^{-1} (dotted lines). (b) Simulated frequency response for TAP detectors with alternating gain and absorption for different values of the net gain per period ΔG and different number of periods N. ΔG is 1 (full lines), 0.5 (dashed lines), and 2 (dotted lines).

two smaller elements, one providing gain and one absorption. In other words, a TAP detector with vertical coupling may be treated as a TAP detector with alternating gain and absorption featuring an arbitrarily large number of periods of very short length each.

Although the contribution to the total background current from absorption of spontaneous emission may be much smaller than the contribution from absorption of ASE in TAP detectors with vertical coupling [38], we believe this to happen only when amplifier modes experience relatively large net gain. In fact, we believe that it is the competition between ASE and spontaneous emission for the electron–hole pairs available for recombination that makes this happen. In other words, in the most interesting operating point where the net modal gain approaches zero for amplifier modes, the contribution from spontaneous emission to the background current in TAP detectors with vertical coupling is far from negligible. A configuration featuring alternating gain and absorption significantly reduces this contribution to the background current. This reduction stems from the much smaller solid angle of absorption region subtended from any point in the amplification region, device length being in the order of a few hundreds of microns, while the width and thickness of the active regions are on the order of a few microns and a few hundreds of nanometers, respectively.

The superior microwave propagation performance is a direct consequence of the signal-carrying electrode being deposited mostly over the insulator as shown in Fig. 8(a). This electrode has a relatively small periodic interaction with doped semiconductor layers, typically for about 10% of its total length. Distributed photocurrent simulations have shown this interaction to produce characteristic impedance close to 50 Ω, small velocity mismatch between electrical and optical velocities ,and small microwave propagation loss [34], not too differently from the case of velocity-matched photodetectors (VMPDs) [10]. Fig. 11 shows the simulated high-speed performances of both configurations, clearly proving this advantage. The frequency response is plotted for different values of the net modal gain per unit length Δg and for different device lengths L in the case of TAP detectors with vertical coupling in Fig. 11(a) as well as different values of the net gain per period ΔG and different numbers of periods N in the case of TAP detectors with alternating gain and absorption in Fig. 11(b). Δg is defined as the net rate of change in the optical power per unit length, while ΔG is the ratio between the optical powers arriving at the beginning of two consecutive device periods. Both parameters are assumed to be constant throughout the entire device. All periods in the TAP detector with alternating gain and absorption are assumed to be identical, and their length is set at 50 μm. Details of the simulated structures are contained in [60]. Fig. 12 plots the simulated response of TAP detectors with alternating gain and absorption presenting a 50-Ω terminated input where photocurrent contributions collected at both the input and output are added. This comparison allows us to determine the bandwidth-limiting

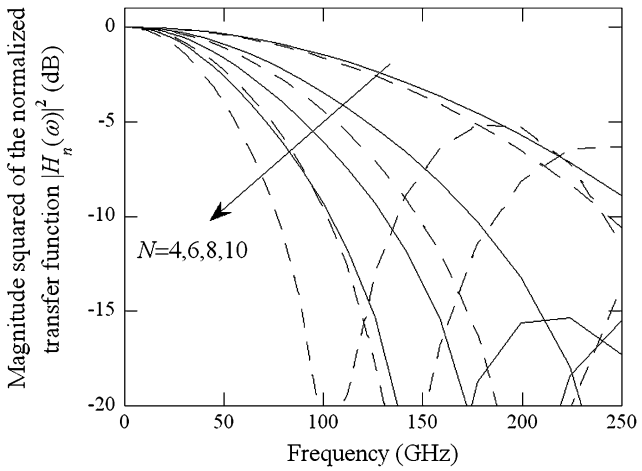

Fig. 12. Simulated frequency responses for TAP detectors with alternating gain and absorption featuring 50 Ω-terminations at input and output, for different values of the net gain per period ΔG and different number of periods N. ΔG is 1 (full lines), 0.5 (dashed lines) and 2 (dotted lines).

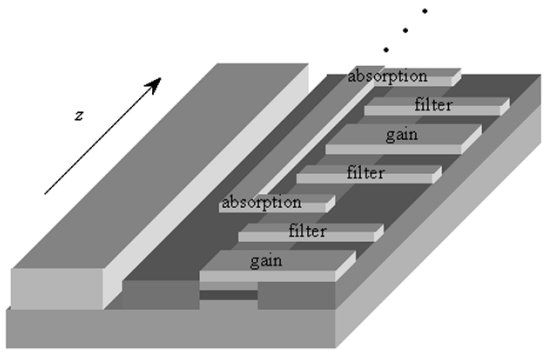

Fig. 13. Schematic representation of a TAP detector with alternating gain and absorption and integrated ASE filtering. Filter sections may consist of absorptive material of slightly larger bandgap than the amplification and detection active regions.

factors in this configuration. It is noteworthy that two different features are shown in the frequency response: a slow rolloff (due to microwave propagation loss), together with the presence of quasi-periodic dips, generated by the addition in and out of phase of the forward- and backward-traveling photocurrent contributions generated at each absorption section. The improvement obtained with the 50-Ω terminated input is a clear consequence of the reduction in the phase delay of the backward-traveling contribution, which is now collected at the input instead of being reflected and traveling all along the device to its output. The optimum device performance at this point occurs for a "balanced" contribution from all absorption sections, i.e., when the power arriving to each detection section is the same, as opposed to an imbalance toward a greater contribution close to the input (for net optical loss in each period) or close to the output (when each period provides net gain), results in a larger fraction of the photocurrent suffering nonconstructive interference due to a larger relative phase delay caused by the path difference between forward- and backward-traveling contributions. We may therefore conclude that, due to the reduced periodic interaction between the photocurrent-carrying electrode and doped semiconductor layers, TAP detectors with alternating gain and absorption do not suffer the effects of microwave propagation loss as severely as TAP detectors with vertical coupling, allowing for much larger device bandwidths. Finally, note that, from the 3-dB bandwidth values extracted from Figs. 11 and 12, efficiency-bandwidth products in the order of 1 THz are possible with external quantum efficiency values in the order of 10, which are indeed possible using this configuration.

Finally, the possibility of introducing integrated optical filtering in TAP detectors with alternating gain and absorption, and the ensuing advantages, will be now addressed. Fig. 13 shows a proposed configuration to achieve this goal in practice. The filtering sections may be implemented, for example, using absorptive material of a slightly larger bandgap than the gain and absorption regions. The purpose of this material is absorbing an important fraction of the ASE photons generated in each amplification section, more specifically most of those whose energy is larger than the bandgap of the filtering active region. Therefore, significant amounts of ASE are produced only in the frequency range between the bandgap of the filtering region and the emission edge of the amplification active material, which may be much narrower than the spontaneous emission spectrum of the gain medium. Since the ASE generated in each gain section accumulates and gets amplified throughout the different periods of the device, this scheme may produce a very significant reduction in the total ASE generated. This would result not only in a lower background current generated in each absorption section from ASE produced in the immediately neighboring gain sections, but also in a much slower overall ASE buildup along the device. The input signal, being of a wavelength intermediate between the band edges of absorption and filtering active regions, would suffer a very small attenuation in each filtering section, resulting in a slightly reduced actual efficiency. However, the significantly lower background current due to ASE absorption more than compensates for this small reduction, for different reasons. First, the signal to background ratio severely increases. Next, the effect of competition between signal and ASE is largely reduced, not only because a much smaller fraction of that ASE is now absorbed, resulting in a much less important decrease of the background current for the same ASE power reduction, but also because the much slower ASE buildup delays saturation of the amplification region to much higher values of the net gain per period, the effect being dramatically reduced in operating points close to cancellation between gain, absorption, and loss for the input signal wavelength in each period. Thus, the measurable photocurrent approaches the value of the photocurrent actually generated by the distributed amplification and absorption of the input signal, and this is true for a much larger range of input optical powers, resulting in a larger measurable efficiency, constant over a wider range of the input optical power. Finally, noise generation decreases, due to a dramatic reduction in the classically denoted spontaneous–spontaneous beat noise term, generated by the absorption of ASE subject to random amplification. The combination of these factors may result in a dramatic improvement in the spurious-free dynamic range (SFDR) of TAP detectors through the introduction of integrated optical filtering, which is possible using state-of-the-art intermixing techniques.

D. Noise in TAP Detectors With Alternating Gain and Absorption

Before establishing the concluding remarks, it is necessary to provide at least a brief description of noise properties of TAP detectors. Using a new particle-like noise model that we have developed for devices featuring a distributed combination of optical amplification and photodetection [60], [61], the noise figure of TAP detectors and the main factors influencing it may be calculated. The new noise model is based on calculating the evolution of the moments of the photon and electron number probability distributions, similarly as the photon statistics master equation [62] calculates the evolution of the photon number probability distribution itself. Both models produce thus equivalent descriptions of the optical noise generated through the amplification process. The photocurrent noise may be described through the electron number variance, which may, in turn, be calculated from the correlation between electron and photon numbers. The new model describes also the evolution of these two quantities, allowing us to calculate the signal-to-noise ratio (SNR) for the output photocurrent as the ratio between the square of the average electron number and the electron number variance. Evaluating in a similar way the input optical SNR, the noise figure for the device may be calculated as a function of the device operating point and of the input optical power.

Using the new noise model, we found an interesting tradeoff: when the net gain per period is close to 1, the noise figure is roughly equal to 2/3 of the external quantum efficiency. This is only true when the input coupling efficiency is close to 100% (no additional partition noise is introduced at the device input), and the spontaneous–spontaneous beat noise term may be neglected in front of the signal-spontaneous beat noise term, i.e., when the photocurrent is much larger than the background current. Deviating from this situation results in a larger noise figure than the minimum value expressed through this proportionality relation.

Figs. 14 and 15 show the noise figure of TAP detectors calculated using the new noise model and assuming full inversion in the gain medium. It is very important to realize the effect of the efficiency of each individual detection section $\eta^{(1)}$ in the overall noise figure. This efficiency is defined as the photocurrent generated in each absorption section, expressed in electrons per unit time, divided by the optical signal power that arrives to it, expressed in photons per unit time. Fig. 14 shows the noise figure in TAP detectors with alternating gain and absorption as a function of the efficiency of each detection section and for different input optical powers, assuming that the device response is linear, i.e., neglecting saturation and competition between signal and ASE, and assuming that actual and measurable efficiencies are equal. More exactly, it shows the noise figure in the particular case where gain, absorption, and loss exactly cancel out in each period, resulting in the same optical power arriving to each detection section. The gain of each amplification section is assumed to be modified by changing bias current into the gain diode in order to achieve this operating condition for the different values of the efficiency of each section. Note that there is a minimum in the noise figure for a value efficiency of each

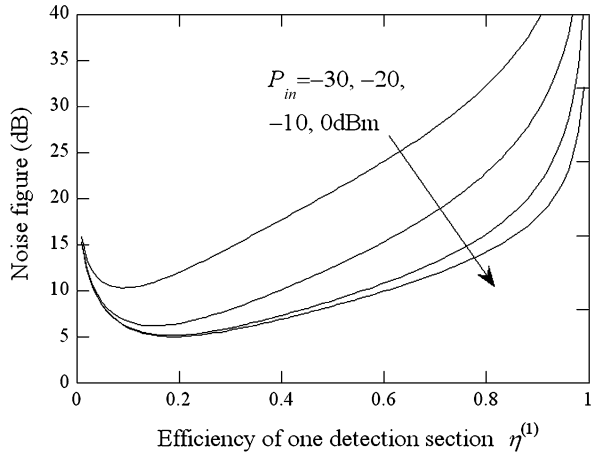

Fig. 14. Noise figure for a TAP detector with alternating gain and absorption as a function of the efficiency of each detection section and for different input optical powers when the net gain per period is 1. Input coupling efficiency is 50%, and the device consists of $N = 6$ periods. First section in the device provides absorption (there is no initial gain section).

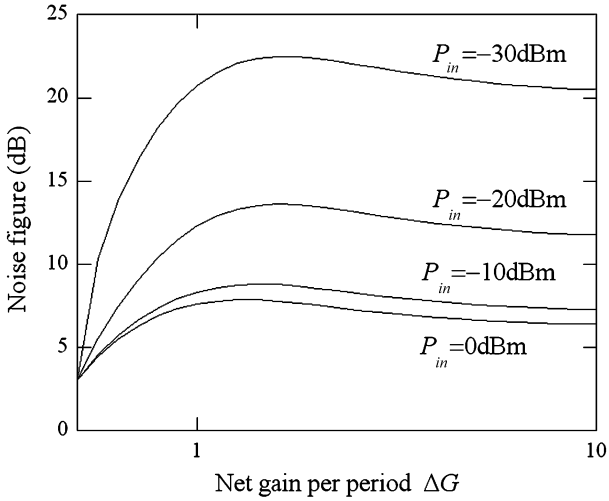

Fig. 15. Noise figure for a TAP detector with alternating gain and absorption as a function of the net gain per period and for different input optical powers when the efficiency of each detection section is 50%. Input coupling efficiency is 50%, and the device consists of $N = 6$ periods. First section in the device provides absorption (there is no initial gain section).

detection section that depends on the input optical power. When the efficiency of each absorption region is close to one, the amount of optical power surviving each detection region is very small, resulting in a large amount of partition noise. When the efficiency of each detection section is close to zero, the gain section needs to be biased just above transparency to achieve net gain per period equal to one (constant optical power arriving to each absorption section). A very small amount of photocurrent is generated, while spontaneous emission is produced and absorbed, resulting in a large amount of spontaneous–spontaneous beat noise relative to the photocurrent. For intermediate values of the efficiency of each detection section, the signal-spontaneous beat noise term dominates. The relative magnitude of this latter term with respect to the spontaneous–spontaneous beat noise contribution depends on the input optical power. Since the spontaneous–spontaneous

and signal-spontaneous noise terms depend differently on the efficiency of each absorption section, different input optical powers correspond to different values of this efficiency for which the minimum noise figure is obtained. It also becomes apparent that integrated optical filtering (not considered in the simulation results shown in Figs. 14 and 15) is necessary to allow for the device noise figure to approach its optimum value. This optimization would be a result of the reduction of the spontaneous–spontaneous beat noise term.

Fig. 15 shows the noise figure as a function of the net gain per period, for an efficiency of each absorption section featuring a realistic value of 50%. The value of the net gain per period for which the noise figure drops to zero corresponds to a zero bias current injected in the amplifier, hence no spontaneous emission or ASE is produced. It is noteworthy that when the bias current injected into the gain diode reaches realistic values, the noise figure is a relatively flat function of the net gain per period. In other words, as the net gain per period raises above one, the performance of TAP detectors becomes similar to that of a semiconductor optical amplifier (SOA) followed by a traditional photodiode, since an increasingly larger fraction of the total photocurrent is produced in the last absorption section, where the arriving optical power is maximum. Therefore, biasing the amplification regions such that the net gain per period is just above one, we may obtain a large external quantum efficiency (in the order of 1000%), a large bandwidth (in the order of 100 GHz) while maintaining a noise figure similar to that of traditional SOAs. Note that in Figs. 14 and 15 the effect of the input coupling loss (assumed to be 50%) in the total noise figure is already taken into account and that the first active section in the device is an absorption section (the first gain section shown in Figs. 8(a) and 13 is assumed not to exist in this case). The noise figure of TAP detectors may be decreased by introducing a longer independently biased first gain section before the first absorption section. This approach also contributes to enhance the external quantum efficiency, allowing for multiterahertz bandwidth-efficiency products with 6–8-dB noise figures, while the optical power inside the device never grows beyond ten times the input optical power.

IV. Conclusion

In summary, we have reviewed our recent work on TWPD with ultrahigh power–bandwidth and gain–bandwidth products performance. By utilizing the superior microwave guiding structure of MSM-TWPD and the short carrier-trapping time of LTG-GaAs-based photoabsorption layer, record high power–bandwidth product performances have been demonstrated under short and long wavelength excitation. Different nonlinear behaviors in these two wavelength regimes have been observed under high-power illuminations. Compared with the bandwidth degradation behavior of short excitation wavelengths (~800 nm), the saturation behaviors under long wavelength excitation are more serious and can be attributed to more serious hot electron and intervalley scattering effect of photogenerated carriers with high excess energy (~300 meV). By using the edge-coupled MSM-TWPD with its superior microwave guiding properties, we have also demonstrated a novel membrane terahertz photonic transmitter without the integration with Si lenses and attained record high optical-to-terahertz power conversion efficiency ($\sim 1.1\times 10^{-3}$) at 650 GHz under pulse mode operation condition.

We have also shown experimental results on a novel device, the traveling-wave amplifier photodetector, presenting external quantum efficiency in excess of 200% at short wavelength (850 nm) and in excess of 100% at long wavelength (1.55 μm). We have also proposed the fabrication of these devices in a configuration presenting alternating optical gain and absorption, which could improve their efficiency and linearity, through the introduction of integrated optical filtering, while at the same time allowing for higher frequency response (bandwidth in the order of 100 GHz). An optimized configuration would furthermore feature an initial amplification section with a double purpose, i.e., further enhancement of the external efficiency and reduction of the noise figure.

References

[1] J. E. Bowers and C. A. Burrus, "Ultrawide-band long-wavelength p-i-n photodetectors," *J. Lightwave Technol.*, vol. LT-5, pp. 1339–1350, Oct. 1987.

[2] K. Kato, "Ultrawide-band/high-frequency photodetectors," *IEEE Trans. Microwave Theory Tech.*, vol. 47, pp. 1265–1281, July 1999.

[3] M. Gokkavas, B. M. Onat, E. Ozbay, E. P. Ata, J. Xu, E. Towe, and M. S. Unlu, "Design and optimization of high-speed resonant cavity enhanced schottky photodiodes," *IEEE J. Quantum Electron.*, vol. 35, pp. 208–215, Feb. 1999.

[4] K. Kato, S. Hata, A. Kozen, J. Yoshida, and K. Kawano, "Highly efficient 40 GHz waveguide InGaAs p-i-n photodiode employing multimode waveguide structure," *IEEE Photon. Technol. Lett.*, vol. 3, pp. 820–822, Sept. 1991.

[5] K. Kato, A. Kozen, Y. Muramoto, Y. Itaya, T. Nagatsuma, and M. Yaita, "110-GHz, 50% efficiency mushroom-mesa waveguide p-i-n photodiode for a 1.55 μm wavelength," *IEEE Photon. Technol. Lett.*, vol. 6, pp. 719–721, 1994.

[6] H. F. Taylor, O. Eknoyan, C. S. Park, K. N. Choi, and K. Chang, "Traveling wave photodetectors," *Optoelectron. Signal Processing Phased-Array Antennas II*, pp. 59–63, 1990.

[7] K. S. Giboney, M. J. W. Rodwell, and J. E. Bowers, "Travelling-wave photodetectors," *IEEE Photon. Technol. Lett.*, vol. 4, pp. 1363–1365, Dec. 1992.

[8] G. A. Vawter and V. M. Hietala, "Unlimited-bandwidth distributed optical phase modulators and detectors: Design and fabrication issue," in *Proc. Int. 1994 IEEE MTT-S Topical Meet. Optical Microwave Interactions*, Nov. 21–23, 1994, pp. 3–6.

[9] C. L. Goldsmith, G. A. Magel, B. M. Kanack, and R. J. Baca, "Coherent combing of RF signals in a traveling-wave photodetector array," *IEEE Photon. Technol. Lett.*, vol. 9, pp. 998–990, July 1997.

[10] L. Y. Lin, M. C. Wu, T. Itoh, T. A. Vang, R. E. Muller, D. L. Sivco, and A. Y. Cho, "Velocity-matched distributed photodetectors with high saturation power and large bandwidth," *IEEE Photon. Technol. Lett.*, vol. 8, pp. 1376–1378, Oct. 1996.

[11] H. Nie, K. A. Anselm, C. Lenox, P. Yuan, C. Hu, G. Kinsey, B. G. Streetman, and J. C. Campbell, "Resonant-cavity separate absorption, charge and multiplication avalanche photodiodes with high-speed and high gain-bandwidth product," *IEEE Photon. Technol. Lett.*, vol. 10, pp. 409–411, Mar. 1998.

[12] G. S. Kinsey, J. C. Campbell, and A. G. Dentai, "Waveguide avalanche photodiode operating at 1.55 μm with a gain-bandwidth product of 320 GHz," *IEEE Photon. Technol. Lett.*, vol. 13, pp. 842–844, Aug. 2001.

[13] J. Wei, F. Xia, and S. R. Forrest, "A high-responsivity high-bandwidth asymmetric twin-waveguide coupled InGaAs-InP-InAlAs avalanche photodiode," *IEEE Photon. Technol. Lett.*, vol. 14, pp. 1590–1592, Nov. 2002.

[14] W. Wu, A. R. Hawkins, and J. E. Bowers, "Design of silicon hetero-interface photodetectors," *J. Lightwave Technol.*, vol. 15, pp. 1608–1615, Aug. 1997.

[15] Y. Kang, P. Mages, A. R. Clawson, P. K. L. Yu, M. Bitter, Z. Pan, A. Pauchard, S. Hummel, and Y. H. Lo, "Fused InGaAs-Si avalanche photodiodes with low-noise performances," *IEEE Photon. Technol. Lett.*, vol. 14, pp. 1593–1595, Nov. 2002.

[16] T. Nakata, T. Takeuchi, I. Watanabe, K. Makita, and T. Torikai, "10 Gb/s high sensitivity, low-voltage-operation avalanche photodiodes with thin InAlAs multiplication layer and waveguide structure," *Electron. Lett.*, vol. 36, pp. 2033–2034, Nov. 2000.

[17] S. Hanatani, M. Shishikura, S. Tanaka, H. Kitano, T. Miyazaki, and H. Nakamura, "A strained InAlAs/InGaAs superlattice avalanche photodiode for operation at an IC-power-supply voltage," in *Proc. Int. Conf. Indium Phosphide Related Materials 1995*, May 1995, pp. 369–372.

[18] T. Nakata, T. Takeuchi, K. Makita, and T. Torikai, "High-speed and high-sensitivity waveguide InAlAs avalanche photodiodes for 10–40 Gb/s receivers," in *Proc. IEEE Lasers Electro-Optics Soc. 2001 Ann. Meeting*, Nov. 2001, pp. 770–771.

[19] S. Demiguel, X. Zheng, N. Li, X. Li, J. C. Campbell, J. Decobert, N. Tscherptner, and A. Anselm, "High-responsivity and high-speed evanescently-coupled avalanche photodiodes," *Electron. Lett.*, vol. 39, Dec. 2003.

[20] N. Shimizu, N. Watanabe, T. Furuta, and T. Ishibashi, "InP-InGaAs unitraveling-carrier photodiode with improved 3-dB bandwidth of over 150 GHz," *IEEE Photon. Technol. Lett.*, vol. 10, pp. 412–414, Mar. 1998.

[21] H. Ito, T. Furuta, S. Kodama, N. Watanabe, and T. Ishibashi, "Inp/InGaAs uni-travelling-carrier photodiode with 310 GHz bandwidth," *Electron. Lett.*, vol. 36, pp. 1809–1810, Oct. 2000.

[22] S. Jasmin, N. Vodjdani, J. Renaud, and A. Enard, "Diluted- and distributed-absorption microwave waveguide photodiodes for high efficiency and high power," *IEEE Trans. Microwave Theory Tech.*, vol. 45, pp. 1337–1341, Aug. 1997.

[23] V. M. Hietala, G. A. Vawter, T. M. Brenan, and B. E. Hammons, "Traveling-wave photodetectors for high-power, large bandwidth applications," *IEEE Trans. Microwave Theory Tech.*, vol. 43, pp. 2291–2297, Sept. 1995.

[24] J.-W. Shi and C.-K. Sun, "Design and analysis of long-absorption length traveling-wave photodetector," *J. Lightwave Technol.*, vol. 18, pp. 2176–2187, Dec. 2000.

[25] Y. Hirota, T. Ishibashi, and H. Ito, "1.55-μm wavelength periodic traveling-wave photodetector fabricated using unitraveling-carrier photodiode structures," *J. Lightwave Technol.*, vol. 19, pp. 1751–1758, Nov. 2001.

[26] A. Stohr, R. Heinzelmann, C. Kaczmarek, and D. Jager, "Ultra-broadband $\mathrm{K_a}$ to W-band 1.55 μm traveling-wave photomixer," *Electron. Lett.*, vol. 36, pp. 970–972, May 2000.

[27] J.-W. Shi, K. G. Gan, Y. J. Chiu, Y.-H. Chen, C.-K. Sun, Y. J. Yang, and J. E. Bowers, "Metal-semiconductor-metal traveling-wave-photodetectors," *IEEE Photon. Technol. Lett.*, vol. 13, pp. 623–625, June 2001.

[28] J.-W. Shi, K. G. Gan, Y.-H. Chen, C.-K. Sun, Y. J. Chiu, and J. E. Bowers, "Ultra-high power-bandwidth product and nonlinear photo-conductance performances of low-temperature-grown GaAs based metal-semiconductor-metal traveling-wave photodetectors," *IEEE Photon. Technol. Lett.*, vol. 14, pp. 1587–1589, Nov. 2002.

[29] J.-W. Shi, Y.-H. Chen, K.-G. G, Y.-J. Chiu, C.-K. Sun, and J. E. Bowers, "High speed and high power performances of LTG-GaAs based metal-semiconductor-metal traveling-wave-photodetectors in 1.3 μm wavelength regime," *IEEE Photon. Technol. Lett.*, vol. 14, pp. 363–365, Mar. 2002.

[30] J.-W. Shi, Y.-H. Chen, K. G. Gan, Y. J. Chiu, J. E. Bowers, M.-C. Tien, T.-M. Liu, and C.-K. Sun, "Nonlinear behaviors of low-temperature-grown GaAs-based photodetectors around 1.3-μm telecommunication wavelength," *IEEE Photon. Technol. Lett.*, vol. 16, pp. 242–244, Jan. 2004.

[31] C.-K. Sun, Y.-H. Chen, J.-W. Shi, Y.-J. Chiu, K. G. Gan, and J. E. Bowers, "Electron relaxation and transport dynamics in low-temperature-grown GaAs under 1 eV optical excitation," *Appl. Phys. Lett.*, vol. 83, pp. 911–913, Aug. 2003.

[32] J.-W. Shi, S.-W. Chu, M.-C. Tien, C.-K. Sun, Y. J. Chiu, and J. E. Bowers, "Edge-coupled membrane THz photonic transmitter based on metal-semiconductor-metal traveling-wave photodetectors," *Appl. Phys. Lett.*, vol. 80, pp. 5108–5110, Dec. 2002.

[33] M.-C. Tien, H.-H. Chang, J.-Y. Lu, L.-J. Chen, S.-Y. Chen, R.-B. Wu, W.-S. Liu, J.-I. Chyi, and C.-K. Sun, "Device saturation behavior of submillimeter-wave membrane photonic transmitters," *IEEE Photon. Technol. Lett.*, vol. 16, pp. 873–875, Mar. 2004.

[34] D. Lasaosa, Y. J. Chiu, J. Piprek, and J. E. Bowers, "Traveling-wave amplification photodetector (TAP detector)," in *Proc. 13th Ann. Meeting IEEE Lasers and Electro-Optics Soc. (LEOS)*, vol. 1, 2000, pp. 260–261.

[35] ——, "Modeling of traveling-wave amplification photodetectors (TAP detectors)," in *Proc. SPIE-Photonics West Int. Symp.*, vol. 4283, 2001, pp. 528–539.

[36] J. Piprek, D. Lasaosa, D. Pasquariello, and J. E. Bowers, "Physics of waveguide photodetectors with integrated amplification," in *Proc. SPIE-Photonics West Int. Symp.*, vol. 4986, 2003.

[37] ——, "Optimization of GaAs amplification photodetectors for 700% quantum efficiency," *IEEE J. Select. Topics Quantum Electron.*, vol. 9, pp. 776–782, May/June 2003.

[38] D. Lasaosa, D. Pasquariello, J. Piprek, and J. E. Bowers, "Recent advances in photodetectors with distributed optical amplification," in *Proc. SPIE-ITCom Int. Symp.*, vol. 5246, 2003.

[39] J. Piprek, D. Pasquariello, D. Lasaosa, and J. E. Bowers, "1.55 μm traveling-wave amplification photodetector," in *Proc. Int. Conf. Indium Phosphide and Related Materials (IPRM)*, 2003, pp. 499–501.

[40] D. Pasquariello, J. Piprek, D. Lasaosa, and J. E. Bowers, "InP-based waveguide photodetector with integrated photon multiplication," in *Proc. SPIE-ITCom Int. Symp.*, vol. 5248, 2003.

[41] K. C. Gupta, R. Garg, I. Bahl, and P. Bhartia, *Microstrip Lines and Slotlines*. Boston, MA: Artech, 1996.

[42] K. J. Weingarten, M. J. W. Rodwell, and D. M. Bloom, "Picosecond optical sampling of GaAs integrated circuits," *IEEE J. Quantum Electron.*, vol. 24, pp. 198–220, 1988.

[43] Y. J. Chiu, S. B. Fleischer, and J. E. Bowers, "High-speed low-temperature-grown GaAs p-i-n traveling-wave photodetector," *IEEE Photon. Technol. Lett.*, vol. 10, pp. 1012–1014, July 1998.

[44] Y. J. Chiu, S. B. Fleischer, J. E. Bowers, A. C. Gossard, and U. K. Mishra, "High-power, high-speed, low-temperature-grown GaAs p-i-n traveling wave photodetector," in *Conf. Lasers Electro-Optics*, May 1998, pp. 501–502. OSA Tech. Dig..

[45] K. G. Gan, J.-W. Shi, Y.-H. Chen, C.-K. Sun, Y. J. Chiu, and J. E. Bowers, "Ultrahigh power-bandwidth-product performance of low-temperature-grown-GaAs based metal-semiconductor-metal traveling-wave photodetectors," *Appl. Phys. Lett.*, vol. 80, pp. 4054–4056, May 2002.

[46] C.-K. Sun, I.-H. Tan, and J. E. Bowers, "Ultrafast transport dynamics of p-i-n photodetectors under high-power illumination," *IEEE Photon. Technol. Lett.*, vol. 10, pp. 135–137, Jan. 1998.

[47] K. S. Giboney, M. J. Rodwell, and J. E. Bowers, "Traveling-wave photodetector design and measurements," *IEEE J. Select. Topics Quantum Electron.*, vol. 2, pp. 622–629, Sept. 1996.

[48] L. Y. Lin, M. C. Wu, T. Itoh, T. A. Vang, R. E. Muller, D. L. Sivco, and A. Y. Cho, "High-power high-speed photodetectors design, analysis, and experiment demonstration," *IEEE Trans. Microwave Theory Tech.*, vol. 45, pp. 1320–1331, Aug. 1997.

[49] Y.-L. Huang and C.-K. Sun, "Nonlinear saturation behaviors of high-speed p-i-n photodetectors," *J. Lightwave Technol.*, vol. 18, pp. 203–212, Feb. 2000.

[50] H. Erlig, S. Wang, T. Azfar, A. Udupa, H. R. Fetterman, and D. C. Streit, "LT-GaAs detector with 451 fs response at 1.55 μm via two-photon absorption," *Electron. Lett.*, vol. 35, pp. 173–174, Jan. 1999.

[51] M. Tani, K.-S. Lee, and X.-C. Zhang, "Detection of terahertz radiation with low-temperature-grown GaAs-based photoconductive antenna using 1.55 μm probe," *Appl. Phys. Lett.*, vol. 77, pp. 1396–1398, Aug. 2000.

[52] N. Zamdmer, Q. Hu, K. A. Mclntosh, and S. Verghese, "Increase in response time of low-temperature-grown GaAs photoconductive switches at high voltage bias," *Appl. Phys. Lett.*, vol. 75, pp. 2313–2315, 1999.

[53] K. A. Mclntosh, E. R. Brown, K. B. Nichols, O. B. McMahon, W. F. DiNatale, and T. M. Lyszczarz, "Terahertz photomixing with diode lasers in low-temperature-grown GaAs," *Appl. Phys. Lett.*, vol. 67, pp. 3844–3846, 1995.

[54] H. Eisele, A. Rydberg, and G. I. Haddad, "Recent advances in the performance of InP Gunn devices and GaAs TUNNET diodes for the 100–300-GHz frequency range and above," *IEEE Trans. Microwave Theory Tech.*, vol. 48, pp. 626–631, Apr. 2000.

[55] Yu. P. Gousev, I. V. Altukhov, K. A. Korolev, V. P. Sinis, M. S. Kagan, E. E. Haller, M. A. Odnoblyudov, I. N. Yassievich, and K.-A. Chao, "Widely tunable continuous-wave THz laser," *Appl. Phys. Lett.*, vol. 75, pp. 757–759, 1999.

[56] R. Kohler, A. Tredicucci, F. Beltram, H. E. Beere, E. H. Linfield, A. G. Davies, D. A. Ritchie, R. C. Iotti, and F. Rossi, "Terahertz semiconductor-heterostructure lasers," in *Conf. Lasers Electro-Optics (CLEO)*, 2002. OSA, postdeadline papers, CPDC12-1.

[57] M. Reddy, S. C. Martin, A. C. Molnar, R. E. Muller, R. P. Smith, P. H. Siegel, M. J. Mondry, M. J. W. Rodwell, H. Kroemer, and S. J. Allen Jr., "Monolithic Schottky-collector resonant tunnel diode oscillator arrays to 650 GHz," *IEEE Electron Device Lett.*, vol. 18, pp. 218–221, 1997.

[58] S. M. Duffy, S. Verghese, K. A. McIntosh, A. Jackson, A. C. Gossard, and S. Matsuura, "Accurate modeling of dual dipole and slot elements used with photomixers for coherent terahertz output power," *IEEE Trans. Microwave Theory Tech.*, vol. 49, pp. 1032–1038, June 2001.
[59] A. W. Jackson, Ph.D. dissertation, Univ. California, Santa Barbara, 1999.
[60] D. Lasaosa, "Traveling-Wave amplifier photodetectors," Ph.D. dissertation, Univ. California, Santa Barbara, 2004.
[61] D. Lasaosa and J. E. Bowers, "New model for the evolution of photon and electron number statistics in the presence of distributed optical amplification and photodetection," , to be published.
[62] K. Shimoda, H. Takahasi, and C. H. Townes, "Fluctuations in amplification of quanta with application to maser amplifiers," *J. Phys. Soc. Japan*, vol. 12, no. 6, p. 686, 1957.

Daniel Lasaosa received the B.E. degree from the Public University of Navarra, Spain, and the M.E. degree from the National Technical Institute in Grenoble, France, both in 1995. He received the M.S. and Ph.D. degrees from the University of California, Santa Barbara, in 1997 and 2004, respectively.

His research interests include traveling-wave photodetectors.

Dr. Lasaosa was a member of the national team representing Spain in the International Mathematical Olympiad in 1990.

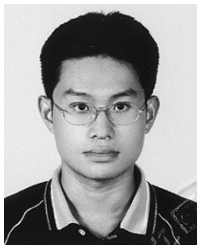

Jin-Wei Shi was born in Kaohsiung, Taiwan, R.O.C., on January 22, 1976. He received the B.S. degree in electrical engineering and the Ph.D. degree in electrooptical engineering, both from National Taiwan University, Taipei, Taiwan, in 1998 and 2002, respectively.

He was a Visiting Scholar at the University of California, Santa Barbara, during 2000 and 2001. In 2002 and 2003, he served as a Postdoctoral Researcher at Electronic Research & Service Organization (ERSO) of Industrial Technology Research Institute (ITRI). Now, he is an Assistant Professor in the Department of Electrical Engineering, National Central University, Taoyuan, Taiwan. His current research interests include ultrahigh-speed/power optoelectronic devices, such as photodetectors, electro-absorption modulator, submillimeter wave photonic transmitters, and semiconductor lasers.

Donato Pasquariello received the Ph.D. degree from the Ångström Laboratory, Uppsala University, Sweden, in 2001, where he worked on micro-opto-electromechanical systems and wafer bonding.

He was a Postdoctoral Researcher at the University of California, Santa Barbara, conducting research on travelling-wave amplifier photodetectors. Currently, he works at Philips Research Laboratories, Eindhoven, The Netherlands, where he is engaged in development of new display technologies.

Kian-Giap Gan was born in Malaysia. He received the B.S. degree in electrical engineering from National Taiwan University, Taipei, Taiwan, R.O.C., in 1999. He is currently working toward the M.S./Ph.D. degree at the University of California, Santa Barbara.

His research interests include the study of high-speed optoelectronic devices and materials.

Ming-Chun Tien was born in Tainan, Taiwan, R.O.C., on May 31, 1979. He received the B.S. degree in electrical engineering and the M.S. degree in electrooptical engineering, both from the National Taiwan University, Taipei, Taiwan, in 2001 and 2003, respectively. He is working toward the Ph.D. degree in electrical engineering at the University of California, Los Angeles.

His research interests include microwave photonics, high-speed optoelectronics devices, and active devices for optical communication.

Hsu-Hao Chang was born in Taipei, Taiwan, R.O.C., in 1978. He received the B.S. degree in electrical engineering from the National Taiwan University, Taipei, Taiwan, in 2000. He is currently working toward the M.S. degree in electrooptical engineering at the same university.

He served in the military in Taiwan for two years. His main research interests include ultrafast optics and terahertz photonic transmitters.

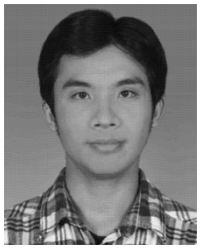

Shi-Wei Chu was born in Taipei, Taiwan, R.O.C., on Oct. 26, 1977. He received the B.S. degree in electrical engineering and the M.S. degree in electro-optical engineering from National Taiwan University, Taipei, Taiwan, in 1999 and 2001, respectively. He is currently working toward the Ph.D. degree in electro-optical engineering at the same university.

He joined the UltraFast Optics Laboratory in 1999 where he was engaged in research on harmonics optical microscopy and terahertz generation under the instruction of Prof. C.-K. Sun. His current research interests include the application of the harmonics optical microscopy to III-nitride semiconductor material, to developmental biology, and to skin biopsy.

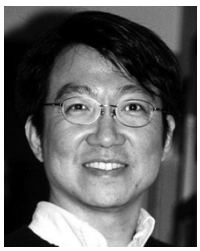

Chi-Kuang Sun (M'96-SM'01) was born in Tainan, Taiwan, R.O.C., in 1965. He received the B.S. degree in electrical engineering from National Taiwan University (NTU), Taipei, Taiwan, in 1987 and the M.S. and Ph.D. degrees in applied physics from Harvard University, Cambridge, MA, in 1990 and 1995, respectively.

He was a Visiting Scientist at the Massachusetts Institute of Technology, between 1992 and 1994, working on femtosecond carrier dynamic studies of semiconductors and metals, and at the University of California, Santa Barbara, from 1995 to 1996, conducting research on quantum dots, GaN, microcavity, and high-speed communication devices and systems. In 1996, he joined the Graduate Institute of Electro-Optical Engineering and Department of Electrical Engineering, NTU, where he is now a Full Professor. He founded the NTU Ultrafast Optics Group and his research interests include nano-acoustics, femtosecond laser technology, terahertz optoelectronics, and biomedical optics.

Dr. Sun is a member of the American Physical Society, a Fellow of the Optical Society of America, and a Fellow of the Royal Microscopical Society. He was the recipient of year 2000 C. N. Yang Outstanding Young Researcher Award from Association of Asian Pacific Physical Society and the 2001 Academia Sinica Research Award for Junior Researchers from Academia Sinica of Taiwan.

Yi-Jen Chiu received the B.S. degree from National Cheng-Kung University, the M.S. degree from National Taiwan University, Taipei, Taiwan, R.O.C., and the Ph.D. degree from the University of California, Santa Barbara, in 1989, 1991, and 1999, respectively.

He is a Professor at the Electrical and Computer Engineering Department at the National Sun Yat-Sen University, Taiwan.

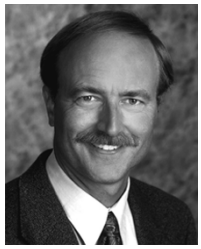

John E. Bowers (F'02) received the M.S. and Ph.D. degrees from Stanford University, Stanford, CA.

He is a Professor in the Department of Electrical Engineering, University of California, Santa Barbara (UCSB). His research interests include optoelectronic devices and optical networking. He is cofounder of the Center for Entrepreneurship and Engineering Management, and a Founder of Terabit Technology and Calient Networks. He worked for AT&T Bell Laboratories and Honeywell before joining UCSB.

Dr. Bowers is a fellow of the OSA and the American Physical Society and a recipient of the IEEE LEOS William Streifer Award.